Applied Clay Science 243 (2023) 107075

Contents lists available at ScienceDirect

Applied Clay Science

journal homepage: www.elsevier.com/locate/clay

Research Paper

Intercalation of carbamide to globular glauconite by chemical processing for the creation of slow-release nanocomposites

Maxim Rudmin [a,b,*], Prokopiy Maximov [a], Evan Dasi [a], Alexander Kurovsky [c], Yana Gummer [c], Kanipa Ibraeva [b], Victor Kutugin [a], Bulat Soktoev [a], Konstantin Ponomarev [b], Evgeny Tararushkin [d], Boris Makarov [a], Alexey Ruban [a]

[a] Tomsk Polytechnic University, 634050 Tomsk, Russia
[b] Institute of Environmental and Agricultural Biology (X-BIO), University of Tyumen, 625003 Tyumen, Russia
[c] Biological Institute, Tomsk State University, 634050 Tomsk, Russia
[d] International Laboratory for Supercomputer Atomistic Modelling and Multi-Scale Analysis, HSE University, 101000 Moscow, Russia

ARTICLE INFO

Keywords:
Glauconite
Carbamide
Nitrogen intercalation
Globules
Potassium
Slow-release fertiliser

ABSTRACT

This article investigates the intercalation of carbamide within globular glauconite involving the chemical activation of glauconite with carbamide solution-gel at varying concentrations of total nitrogen (N). Mineral nanocomposites were prepared with a multitude of novel functions. As the N concentration of the initial solution increased, the proportion of intercalated N enhanced to 8%. A 20% of N concentration in carbamide solution maximizes intercalation. Intercalation occurs in the interlayer of smectite layers (micropores) in glauconite. In nanocomposites, the decrease in specific surface space, total volume pores, and average pore size reflect the absorption of carbamide in meso- and macropores of glauconite globules. Glauconite nanocomposites retain a spherical particle morphology and a distinct microlayer close to the surface. The increased proportion of nitrogen in the microlayers close to the surface indicates a high filtration capacity of the globules. The near-surface microlayer serves as a diffusion channel for the glauconite interior, where new substances are absorbed in the micro- (interlayer) and macropores. The stepwise kinetics of nutrient release, which supports the various forms of carbamide absorption in glauconite, distinguishes the nanocomposites. In addition to N-compounds, glauconite nanocomposites are mineral sources of the available potassium (K) in soils. As a result, chemically manufactured glauconite nanocomposites have some following advantages: the micro-granular mineral form, a permeable inner near-surface microlayer, incubated in micro-, meso-, and macropores N-compounds, and the available K.

1. Introduction

The agro-industry requires controlled-release fertilisers (CRFs) to increase efficiency and environmental safety (Sharma, 1979; Trenkel, 1997; Jariwala et al., 2022; Duan et al., 2023). Controlled-release fertilisers deliver nutrients to plants with prolonged effects to prevent nutrient loss and excessive accumulation in soils, surface water, and groundwater (Oertli, 1980; Trenkel, 2010; Ni et al., 2011; Chen et al., 2017). Nitrogen accumulation is frequently observed with traditional fertilisers, such as urea, ammonium nitrate, and ammonium sulfate (Alrbaihat, 2023). Nitrogen nutrients remaining in the agro-land environment cause harm through denitrification, and greenhouse effects cause the eutrophication of water bodies (Akiyama et al., 2010; IPCC, 2014; Obieze et al., 2019; Xiao et al., 2019). Controlled-release fertilisers aim to reduce environmental risks while simultaneously improving crop yield and quality (Mala et al., 2017; Pereira et al., 2017; Fu et al., 2018; Liu et al., 2023). Given the projected population growth that will require a healthy diet, it is crucial to the global challenge (Tilman et al., 2002; Pretty et al., 2010).

CRFs are based on technologies and the creation of principal components (Fu et al., 2018; Lawrencia et al., 2021; Liu et al., 2022; Duan et al., 2023). Technologies for creating CRFs are categorised into

* Corresponding author at: Tomsk Polytechnic University, 634050 Tomsk, Russia.
E-mail addresses: rudminma@tpu.ru (M. Rudmin), pnm1@tpu.ru (P. Maximov), de01@tpu.ru (E. Dasi), k.ibraeva@utmn.ru (K. Ibraeva), kutugin@tpu.ru (V. Kutugin), bulatsoktoev@tpu.ru (B. Soktoev), k.o.ponomarev@utmn.ru (K. Ponomarev), etararushkin@hse.ru (E. Tararushkin), bim5@tpu.ru (B. Makarov), ruban@tpu.ru (A. Ruban).

https://doi.org/10.1016/j.clay.2023.107075
Received 29 April 2023; Received in revised form 11 July 2023; Accepted 13 July 2023
Available online 20 July 2023

chemical (Chen et al., 2017; Rashid et al., 2021), mechanical (Singla et al., 2020; Zhao et al., 2020; Salimi et al., 2021; Rudmin et al., 2022b) and mechanochemical (Solihin et al., 2011; Borges et al., 2017, 2018, 2022; Said et al., 2018; Rudmin et al., 2019; Alrbaihat et al., 2021, 2022; De Oliveira et al., 2021; AlShamaileh et al., 2022) methods. A key component of CRFs is inhibitor substances or containers whose function is to deliver targeted nutrients to plants (Rahman et al., 2021). Inhibitors can be polymeric (González et al., 2015; Pereira et al., 2015) or organo-polymeric substances (González et al., 2015; Liu et al., 2019; Pogorzelski et al., 2020; Elkhlifi et al., 2021; Komariah et al., 2022; Wang et al., 2022) and various minerals (Hussien et al., 2012; Rashidzadeh and Olad, 2014; Puspita et al., 2017; Borges et al., 2018; Sharma et al., 2021). Among the minerals of primary interest are layered silicates such as smectites (Wu et al., 2003; Abramova et al., 2007; Kim et al., 2011; Borges et al., 2017; Golbashy et al., 2017; Hermida and Agustian, 2019; Rudmin et al., 2022b), kaolinite (Solihin et al., 2011; Hussien et al., 2012; Borges et al., 2015, 2017; Lei et al., 2018; Al-Rawajfeh et al., 2019; Alrbaihat et al., 2021), vermiculite (Mortland et al., 1963; De Oliveira et al., 2021), and glauconite (Rudmin et al., 2019, 2020b, 2022a).

Glauconite is of particular interest to the agricultural industry because it is an independent potassium mineral fertiliser (Karimi et al., 2012; Franzosi et al., 2014; Santos et al., 2016; Shekhar et al., 2017; Oze et al., 2019; Hamed and Abdelhafez, 2020; Praveen et al., 2020). Glauconite is a dioctahedral potassium-containing iron-rich phyllosilicate of the 2:1 interlayer deficient mica group (Bailey, 1980; Odom, 1984; Rieder et al., 1988; Drits, 1997; Guggenheim et al., 2007; V.A. Drits et al., 2010a). Soils containing glauconite have long been known to increase fertility (Mansfield, 1919; McRae, 1972). Subsequently, the influence of glauconite on soil fertility found an explanation in the ion exchange, moisture-holding abilities of the mineral, and its naturally granular morphology (Heckman and Tedrow, 2004; Hamed and Abdelhafez, 2020; Rudmin et al., 2020a; Syrchina et al., 2022; Basak et al., 2023). Glauconite almost always contains some smectite layers, depending on the mature of the mineral (Odin and Matter, 1981; Amorosi et al., 2007; V.A. Drits et al., 2010a; Huggett, 2013; Zviagina et al., 2017). The incubation capacity of glauconite is virtually unstudied in contrast to smectite. Several recent studies have reported the intercalation of nitrogen substances with glauconite, resulting in fertilisers with improved positive effects on plant growth and development (Rudmin et al., 2019, 2020b, 2022a). All previous studies used mechanical activation of glauconite using planetary or ring mills to achieve nitrogen intercalation into mineral particles (Rudmin et al., 2022a). Technological methods for creating glauconite-nitrogen composite fertilisers by activation in a planetary or ring mill (Rudmin et al., 2019, 2020b, 2022a) with the selection of various mineral to urea ratios: 3:1, 1:1, and 2:3 have been reported.

This work aims to comprehensively study the intercalation of nitrogen compounds in globular glauconite during interaction with urea solution to develop effective nanocomposite fertilisers. In this investigation, experiments with stepwise and detailed changes in globular glauconite-carbamide ratios are conducted to evaluate factors for the intercalation of nitrogen compounds into the mineral interlayer.

2. Materials and methods

2.1. Minerals and materials

This study used glauconite from the Karin deposit in Russia. The glauconite concentrate, which involves the activation process, consists of about 85% glauconite and 15% quartz and feldspars. The carbamide (CH_4N_2O) solution gel (Terra Master Ltd., Russia) comprises >25% of nitrogen.

2.2. Chemical and mechanochemical preparation of nanocomposites

All experiments used the globular glauconite concentrate as a potential inhibitor of nitrogen release and a carbamide solution gel as a filling nutrient. The preparation of nanocomposites based on glauconite and carbamide was produced by chemical activation. The chemical method impregnates the globular glauconite fraction in the carbamide solutions with nitrogen concentrations of 20 / 10 / 5 mol% for 48 h until a dry state is reached. The finalised nanocomposites were called Gko80N20, Gko90N10, and Gko95N05, respectively. The nitrogen concentration in the solution was achieved by diluting the carbamide gel solution in distilled water.

2.3. Characterisation of nanocomposites

Characteristics of the prepared nanocomposites were studied using X-ray diffraction (XRD), scanning electron microscopy with energy dispersive X-ray spectroscopy (SEM-EDS), transmission electron microscopy (TEM) with selected area electron diffraction (SAED), Fourier transform infrared spectroscopy (FTIR), differential thermal analysis (thermo-gravimetric analysis and differential scanning calorimetry, TG-DSC) with a quadrupole mass spectrometer and Brunauer–Emmett–-Teller (BET).

Structural modifications of glauconite were examined before and after activation of nanocomposites. The mineralogy of randomly oriented nanocomposites was determined using a Bruker D2 Phase X-ray diffractometer (Billerica, MA, USA) with Cu-Kα radiation at a current of 10 mA and a voltage of 30 kV. A fraction of the composites with <10 μm size was scanned from 4° to 50° 2θ, with a step size of 0.02° at a scanning rate of 1.5 s, divergence slit of 1 mm, the anti-scatter slit of 3 mm, and receiving slit of 0.3 mm. Additionally, the clay fraction (<2 μm) of all composites and the initial fraction was divided out by disaggregation, followed by preparing aqueous suspensions in distilled water, sedimentation over 8–16 h and air drying onto glass slides. Each sample was measured in the air-dried state following placement in a desiccator for 24 h at ~60 °C. Original glauconite was scanning in the ethylene-glycol solvated state. Glauconite and smectite were determined according to the procedures described in (Moore and Reynolds Jr., 1997) and (Hillier, 2003). Quantitative mineralogical analysis of the whole rock data was achieved using Rietveld analysis (Bish and Post, 1993) with PDXL and Siroquant software (Taylor, 1991).

The unit structures and interlayers of glauconite crystallites were studied by JEOL JEM-2100F transmission electron microscopy (TEM) at the Center for Sharing Use “Nanomaterials and Nanotechnologies” of Tomsk Polytechnic University. TEM images were captured in the transmission mode. A drop of nanocomposite suspension was allowed to dry on a copper grid (300 mesh, 3.05 mm in diameter) coated with carbon film before examining it with TEM operated at 200 kV. TEM images were taken at sufficiently thin regions of the specimen.

The FTIR spectra of the nanocomposites were obtained between 4000 and 400 1/cm using an FTIR spectrometer (Shimadzu FTIR 8400S, Kyoto, Japan) with a temperature-controlled high-sensitivity detector (DLATGS) from KBr pellets with a resolution of 4 1/cm to identify the chemical bond functional groups in the prepared nanocomposites.

Thermo-gravimetric and differential scanning calorimetry (TG-DSC) curves of nanocomposites were obtained at temperatures from 30 to 1000 °C using an inert argon atmosphere (flow rate 50 ml per minute) with a heating rate of 10 °C/min on a STA 449 F5 Jupiter microthermal analyser (NETZSCH, Germany) to calculate the weight ratio of intercalations of different phases and to study the thermal degradation.

The TG-DSC analysis was coupled (by a transfer line heated to 250 °C) to a Netzsch TA Quadrupole Mass Spectrometer (QMS) 403C Aeolos for simultaneous detection and quantification of the evolved gases. The analyser was calibrated immediately before experimentation. In addition, a buoyancy baseline calibration was also completed. The mass spectrometer (MS) was operated in electron impact ionisation

mode, with ion monitoring for the mass-to-charge (m/z) ratios from 1 to 50.

The nanocomposites were analysed under TESCAN VEGA 3 SBU scanning electron microscope (Brno, Czech Republic), operating at 10–20 kV accelerating voltage, specimen current of 3–12.2 nA, and a spot diameter of ~2 μm.

Elemental analysis was performed in local areas (more than ten sites) of 3 μm^2 under high vacuum conditions for each carbon-coated nanocomposite by OXFORD X-Max 50 energy-dispersive adapter (High Wycombe, UK), adapting with scanning electron microscope. Samples were studied at 20 kV accelerating voltage and specimen current of 12.2 nA. Elemental composition data was gathered for 120 s or until the signal achieved stability, and a distinct distribution pattern was established. The data were then subjected to processing using the sophisticated Oxford Aztec software.

The Brunauer-Emmett-Teller (BET) method was used to measure the specific surface of the samples using a 3P sync 210 adsorption-specific surface and porosity analyser (Ribori Instrumentation, Germany). The samples were dried at 125 °C for 2 h and degassed in a vacuum for 12 h at 250 °C before the surface space was determined at −196 °C in the range of relative pressures from 0.05 to 0.3. The researchers also determined the average pore size and total pore volume by N2 adsorption-desorption isotherms.

2.4. Soil leaching experiments

To conduct the leaching experiment, dry sandy soil with pH of 5.3 weighing 80 g was mixed with nanocomposites. The nanocomposites were added at a dose equivalent to 380 mg N/kg or 250 mg K/kg of dry soil. The soil mixture was then filled into a PVC tube with a mesh bottom (100 mesh), having an inner diameter of 7 cm and a height of 25 cm. The bottom of the column was modified to accommodate a piece of filter paper (Whatman #42) to collect the leachate. A PVC plug with multiple small holes was installed on the bottom wall to prevent soil loss from the column. The experiment was conducted with three repetitions for each product tested, each set of these repetitions being designated as a "plot."

Throughout the experiment, the soil moisture level was maintained at 75%. At regular intervals (1, 4, 7, 14, 21, 28, 42, and 56 days), 200 ml of deionized water was added slowly to each soil column, and the leached solutions (filtrates) were collected in 50 ml conical flasks. Immediately after collection, the pH, potassium (K^+), ammonium (NH_4^+), and nitrate (NO_3^-) concentrations were determined using the ionometric method. The final plot values were calculated as the average of three replicates. Additionally, the cumulative release curves for potassium (K^+), ammonium (NH_4^+), and nitrate (NO_3^-) were computed.

Statistical analysis of the results was conducted using Microsoft Excel 365. The values were calculated as arithmetic means with standard deviations. To determine significant differences between experiments, the least significant difference (LSD) test at the 0.05 probability level was performed following analyses of variance, which were also followed by the LSD.

3. Results

3.1. Structural characterisations of nanocomposites

X-ray diffractograms of activated nanocomposites (Fig. 1) show basal reflexes of glauconite, carbamide, and quartz impurity. In contrast to the original glauconite, the diffractograms of activated nanocomposites show a new basal reflex 001 relevant to the inter-planar distance of expanding smectite layers in glauconite at 15.6 Å, 15.7 Å and 17.0 Å for nanocomposites Gko95N05, Gko90N10, and Gko80N20, respectively. The first basal maximum increased as the ammonium concentration in the solution and glauconite concentration increased. The diffractogram of the Gko80N20 nanocomposite is determined by the presence of reflexes at 4.0, 3.6, 3.2, 3.0, 2.8, 2.5, 2.2, and 1.8 Å, which are relevant to

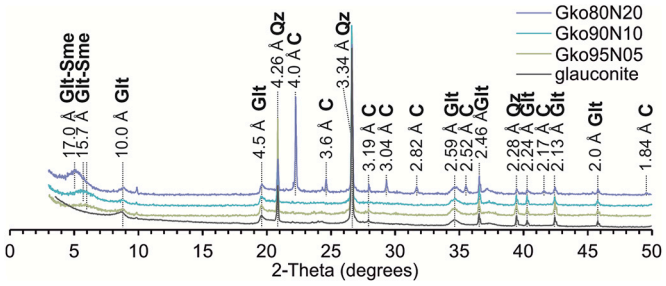

Fig. 1. X-ray patterns of activated nanocomposites and the initial glauconite concentrate. C – carbamide, Glt – glauconite, Glt-Sme – glauconite-smectite, Qz – quartz.

adsorbed carbamide. Glauconite has basal reflexes at 10.0, 4.5, 2.6, 2.45, 2.25, 2.1, and 2.0 Å.

The images with a high resolution (Fig. 2) and patterns of local electron diffraction reveal glauconite nanocomposite particles with enlarged crystal packages. Particles in nanocomposites are typically characterised by an increase of one or two layers of four or five dioctahedral layers (Fig. 2 F). The average interlayer thickness in the original glauconite ranges from 1.9 to 2.7 nm (Fig. 2 C) to 2.2–3.9 nm (Fig. 2 F) in the Gko80N20 nanocomposite.

The IR spectra of the activated nanocomposites (Fig. 3) differ near strain vibrations at 1155, 1452–1462, 1600, 1624, 1680, 3342, and 3442 1/cm. All nanocomposites keep glauconite following vibrations: Si—O at 700, 775, 794, and 1020 1/cm in tetrahedral positions, $Fe^{II}OHFe^{III}$ and $MgOHFe^{III}$ in octahedral positions at 3522 and 3564 1/cm, respectively (Victor A. Drits et al., 2010b; Zviagina et al., 2017). As the fraction of carbamide increases when activated with glauconite, the sharpness of the NH_2 peaks at 1155 and 3442 1/cm, and the NH peaks at 1680 and 3342 1/cm increases. Further, the Gko80N20 nanocomposite exhibits a 1600 1/cm peak relevant to the CO oscillations of absorbed carbamide.

3.2. Composition of nanocomposites

According to EDS analysis, the initial chemical composition of glauconite is the following: 6.8–9.4 wt% K_2O, 18.1–32.9 wt% $Fe_2O_{3\,(total)}$, 50.2–58.2 wt% SiO_2, 3.8–11.8 wt% Al_2O_3, 2.9–4.7 wt% MgO, 0.4–0.6 wt% CaO, 0.3–0.4 wt% Na_2O and 1.7–4.5 wt% LOI (loss on ignition). The crystal-chemical formula is: $K_{0.6–0.8}(Al_{0–0.7}Mg_{0.3–0.5}Fe_{0.9–1.7})_{1.6–2.0}(Si_{3.5–3.8}Al_{0.2–0.6})O_{10}(OH)_2nH_2O$.

The XRD spectrum of air-dried clay fraction of initial glauconite displays a higher-spacing reflection for glauconite (~12.6 Å) according to the 001 basal peaks. The 001 basal reflection splits into various peaks after ethylene-glycol saturation, with the highest intensity at ~10.0 Å and ~ 18.6 Å corresponding to a glauconite-smectite mixed layer. XRD patterns of oriented samples evidence the presence of the expanded smectite phase around 5–10%.

The DSC curve of glauconite has one low acute endothermic effect at 571 °C and one gentle endothermic effect at 122 °C, relevant to quartz admixture and low the process of oxidation of the mineral. In addition, Glauconite is characterised by two flat exothermic effects at 83 and 800 °C, which handle the removal of physically bound water and dehydration of crystal lattice. Thus, the initial glauconite is characterised by four weight loss intervals of 0–110, 110–185, 185–325, 325–590, and 590–100 °C, which relevant to the removal of physically bound water by 0.2 wt%, adsorbed macroporous water by 1. 0 wt%, absorbed mesopore water by 0.6 wt%, interlayer micropore water by 2.4 wt%, and dehydration of dioctahedral crystal meshes by 0.6 wt%, respectively.

The chemical composition of activated glauconite nanocomposites has low differences from the original glauconite. In nanocomposites on glauconite flakes, nitrogen is fixed with the contents up to 1.5%,

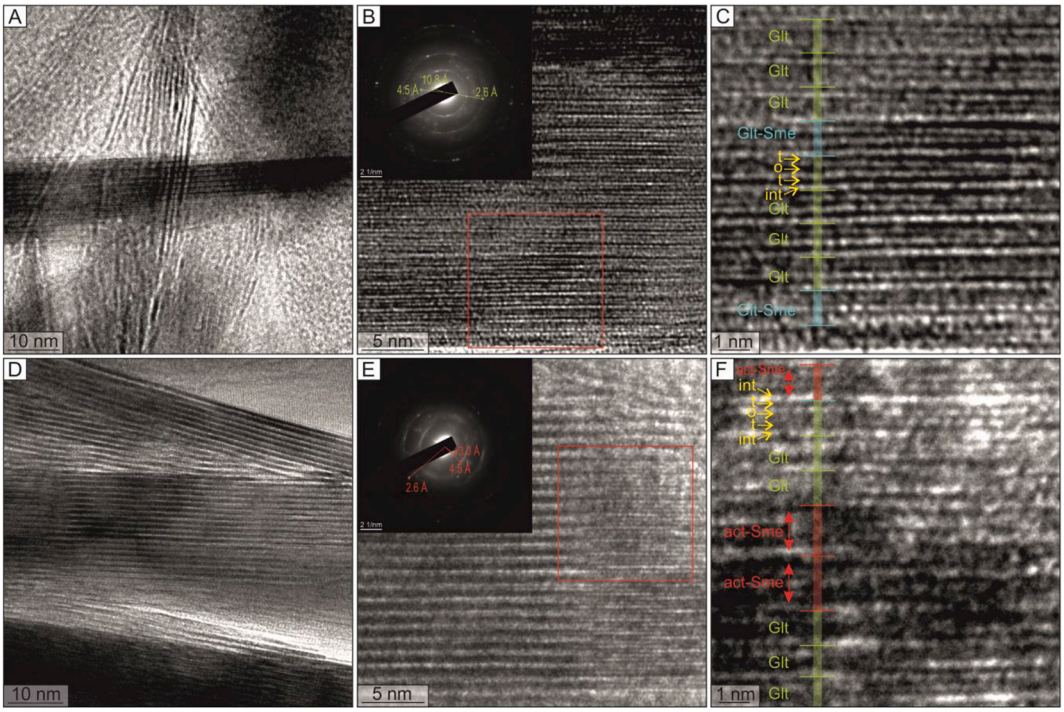

Fig. 2. High-resolution transmission electron microscope images and local electron diffraction patterns (A-C) of the original glauconite and (D—F) of the activated nanocomposite. The maximum magnification image (F) shows a change in the structure of smectite layers in glauconite in the nanocomposite because of the expansion of the interlayer space and crystal package. Glt – glauconite crystalline layers, Glt-Sme – smectite layers in glauconite, act-Sme – nitrogen intercalated in smectite layers of glauconite; t – tetrahedral sheet, o – octahedral sheet, int – interlayer space.

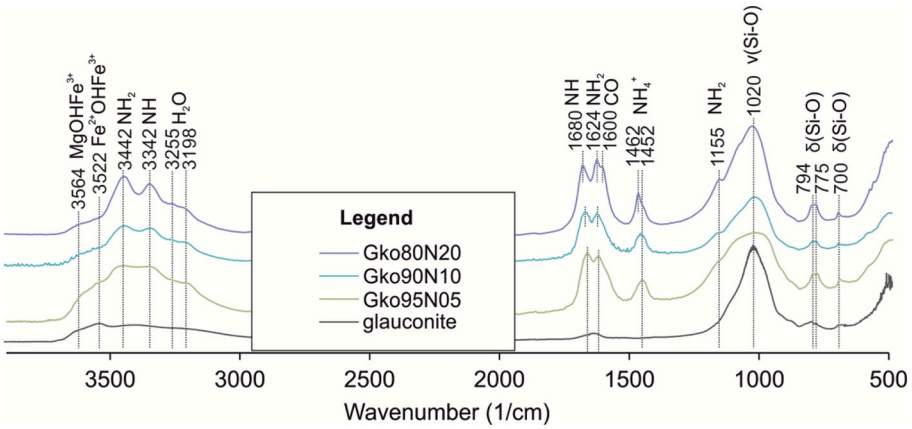

Fig. 3. IR spectra of activated nanocomposites and original glauconite. The sharpness of the 1155 (NH_2), 1680 (NH), 3342 (NH), and 3442 (NH_2) 1/cm peaks increases as the proportion of carbamide in reacted solution increases.

0.9–1.5%, and 1.5–4.5% in Gko95N05, Gko90N10, and Gko80N20, respectively. The content of basic oxides remains stable except for the absence of admixture of Ca and Na on mineral particles.

The DSC curves (Fig. 4A) of nanocomposites Gko95N05 and Gko90N10 show hollow endotherms at 190 and 184 °C, respectively. The Gko80N20 nanocomposite exhibits two acute endothermic effects and one hollow endothermic effect at 134, 188, and 360 °C, respectively, and four hollows exothermic effects at 122, 153 °C, 290, and 650 °C. At 134 °C, the first acute endothermic effect highlights the melting of carbamide. The second endothermic effect at 184–190 °C relevant to the volatilisation of carbamide, specifically NH_3 and CO_2, which is relevant to the absorbed part of the substances added to the mineral. The mild endothermic effect at 360 °C proves the degradation of polymerised part of carbamide. Also, in all nanocomposites, the endothermic effect at 571 °C is preserved, showing a low admixture of quartz.

The TG curves of the nanocomposites (Fig. 4 A) show five major weight loss stages characteristic of glauconite (Table 1): 0–110, 110–185, 185–325, 325–590, 590–1000 °C. The first interval of 0–110 °C is the removal of physically bound water from the mineral at 0.1–0.2 wt%. The second interval, 110–185 °C, is associated with the removal of water and carbamide products (NH_3 and CO_2) from the macropore space of the nanocomposites (Fig. 4 B—D). The weight loss in the second interval is 0.7–3.3 wt%. The third interval, 185–325 °C, covers the release of mesopore water and many carbamide decomposition products, including the following (in order of decreasing ion-current signal intensity): NH_3, CO_2, $HNCO^+$, CO^+, NH^+, NO^+, (Fig. 4 B—D). The weight loss between 185 and 325 °C is 2.1–10.6 wt%. The fourth stage of weight loss is 325–590 °C, in which the weight loss of nanocomposites varies from 2.5 to 8.0%. This stage is associated with removing water and carbamide decomposition products, mainly from

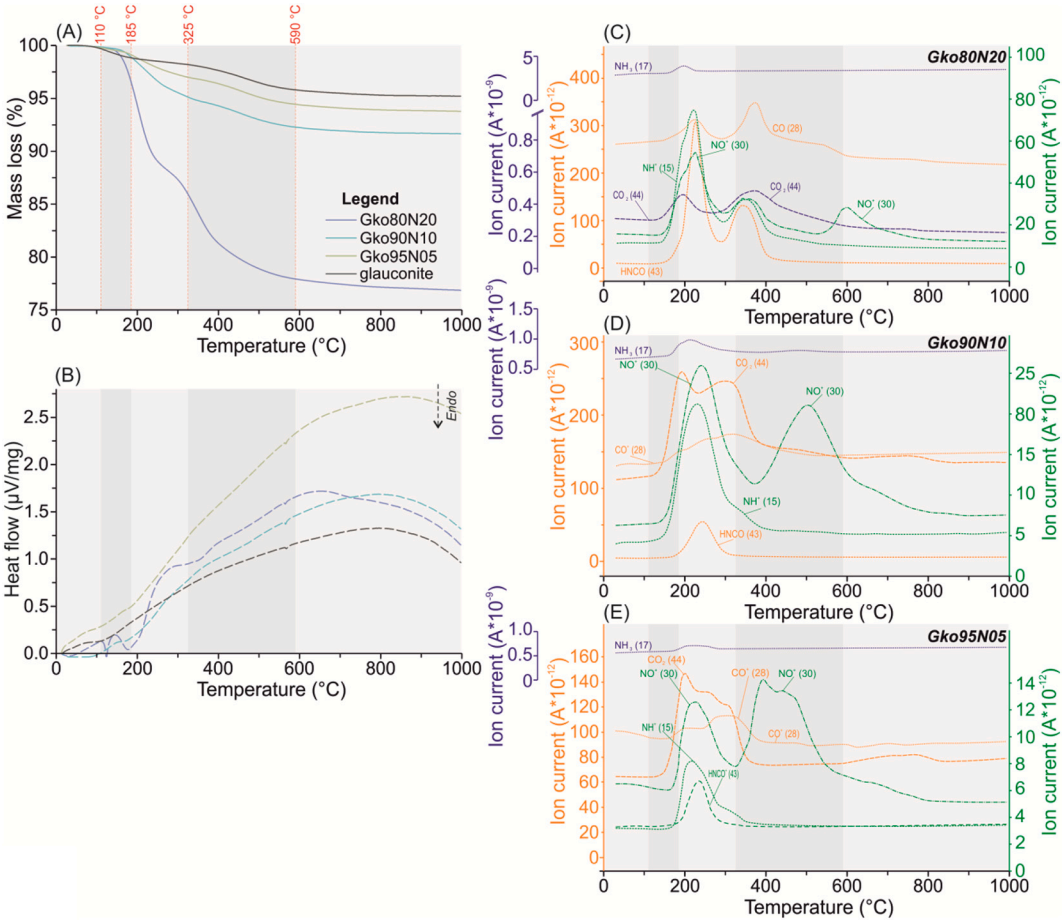

Fig. 4. (A) TGA (solid lines) and DSC curves (dashed lines) of prepared nanocomposites and original glauconite. (B) Selected representative MS multiple ion detection curves (m/z = 15 (NH^+), 17 (NH_3), 28 (CO^+), 30 (NO^+), 43 ($HNCO^+$), 44 (CO_2).

Table 1
Weight losses of glauconite-carbamide nanocomposites and glauconite according to TG analysis.

	Nanocomposites	Weight loss intervals (°C)				
		0–100	100–185	185–325	325–590	590–1000
Weight loss (%)	*Gko95N05*	99.9	99.1	97.0	94.4	93.8
	Gko90N10	99.9	98.9	95.1	92.3	91.7
	Gko80N20	99.9	96.5	86.0	77.9	76.9
	Glauconite	99.8	98.8	98.2	95.8	95.2
Final residue (%)	*Gko95N05*	0.1	0.7	2.1	2.5	0.7
	Gko90N10	0.1	1.0	3.8	2.8	0.6
	Gko80N20	0.1	3.3	10.6	8.0	1.1
	Glauconite	0.2	1.0	0.6	2.4	0.6

the interlayer space of the mineral. This interval recorded the second peak of NO^+ release in all nanocomposites (Fig. 4 B—D). In the Gko80N20 nanocomposite (Fig. 4 B) the release of CO_2, CO, HNCO, NO^+, NH^+ additionally observed. This shows an excessive amount of carbamide in the nanocomposites. In the fifth stage, 590–1000 °C weight loss is 0.6–1.1%, relating to the dehydration of glauconite crystal meshes in nanocomposites.

3.3. Morphology of nanocomposites

The original glauconite and the activated nanocomposites are globular in grain size, ranging from 50 to 250 μm in length (Fig. 5). The internal morphological structure of the globules presented by chaotically oriented microscales with sinuous outlines ranging in size from 0.5 to 2 μm to 4–5 μm in length. The parallel orientation of ultra-micro aggregates that are orthogonal to the surface is one of the characteristics that separates the near-surface layer of glauconite globules. In addition, these microlayers of nanocomposites (Fig. 5 A-D) are differed by an increased amount of nitrogen relative to the core (internal) part of globules.

The specific surface space, pore volume, and average pore size of the original globular glauconite are 41.2 m^2/g, 0.064 cm^3/g, and 8.9 nm, respectively. The specific surface space in nanocomposites (Table 2) decreases as the carbamide fraction during activation increases from 37.9 m^2/g in Gko95N05 to 23.8 m^2/g in Gko80N20. Simultaneously, the average pore volume decreases from 0.061 cm^3/g to 0.036 cm^3/g. The average pore size also decreases to 4.1 nm in the nanocomposite Gko80N20.

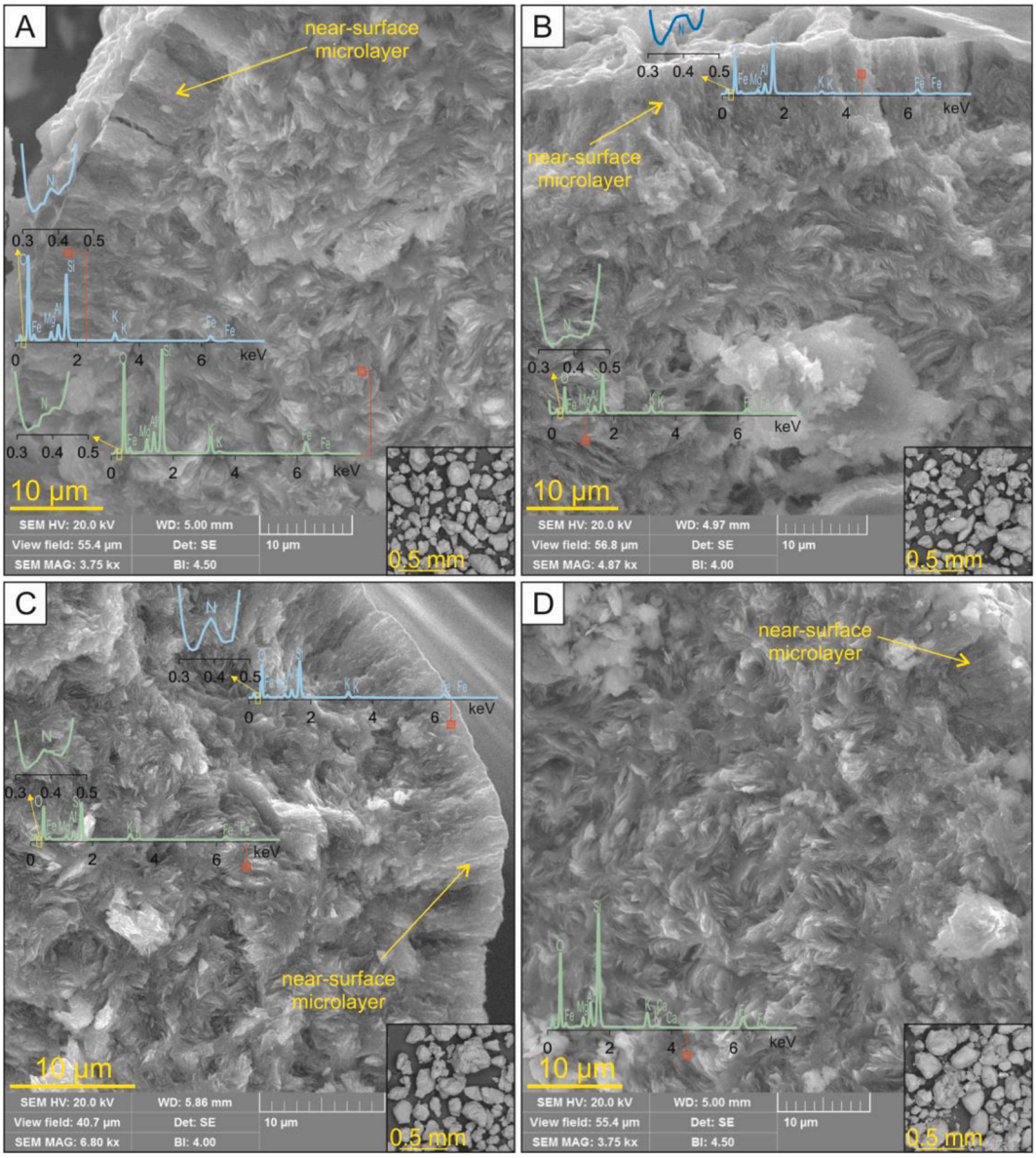

Fig. 5. SEM images in a secondary electron detector showing different morphological features of the nanocomposites (A – Gko95N05, B – Gko90N10, C – Gko80N20) and the original glauconite (D) with EDS spectra in the near-surface microlayers of globules (blue spectra) and in the core part of globules (green spectra). It showed an overview image of the globular fraction of each sample in the lower right corner. The red square is the local accumulation space of the relevant spectrum. (For interpretation of the references to colour in this figure legend, the reader is referred to the web version of this article.)

Table 2
The specific surface area, total pore volume, and average pore size in nanocomposites according to the BET analysis.

Nanocomposites	Surface area (m^2/g)	Total pore volume (cm^3/g)	Average pore diameter (nm)
Gko80N20	23.8	0.036	4.1
Gko90N10	33.2	0.055	6.2
Gko95N05	37.9	0.061	6.4
Glauconite	41.2	0.064	8.9

3.4. Release nutrients from nanocomposites

The laboratory tests yielded different characterisations of the leaching kinetics of ammonium, nitrate, and potassium from nanocomposite cells. Ammonium (Fig. 6 A) has two stages of peak release: days 1–7 and days 21–28. From day 7 to day 21, slow-released ammonium. Therefore, after day 28, the ammonium leaching kinetics are slow and prolonged. Nitrates have relatively high release kinetics in the first seven days (Fig. 6 B), after which they leach minimal amounts to 0.2–0.3 mg between day 7 and day 56. The kinetics of potassium release from the nanocomposites (Fig. 6 C) have four key steps, which differ from the kinetics of potassium leaching from the control cell. The first stage up to day 7 corresponds to a high release rate, the second from day 7 to day 28 has a relatively slow rate, the third from day 28 to day 43 has a maximum release rate, and the fourth from day 43 has a slow kinetics.

4. Discussion

4.1. Structural and morphological features of glauconite-carbamide nanocomposites

Intercalation of beneficial substances within the interlayer space of glauconite is a primary focus in creating effective nanocomposites based on layered minerals. Nitrogen intercalation in glauconite (Rudmin et al.,

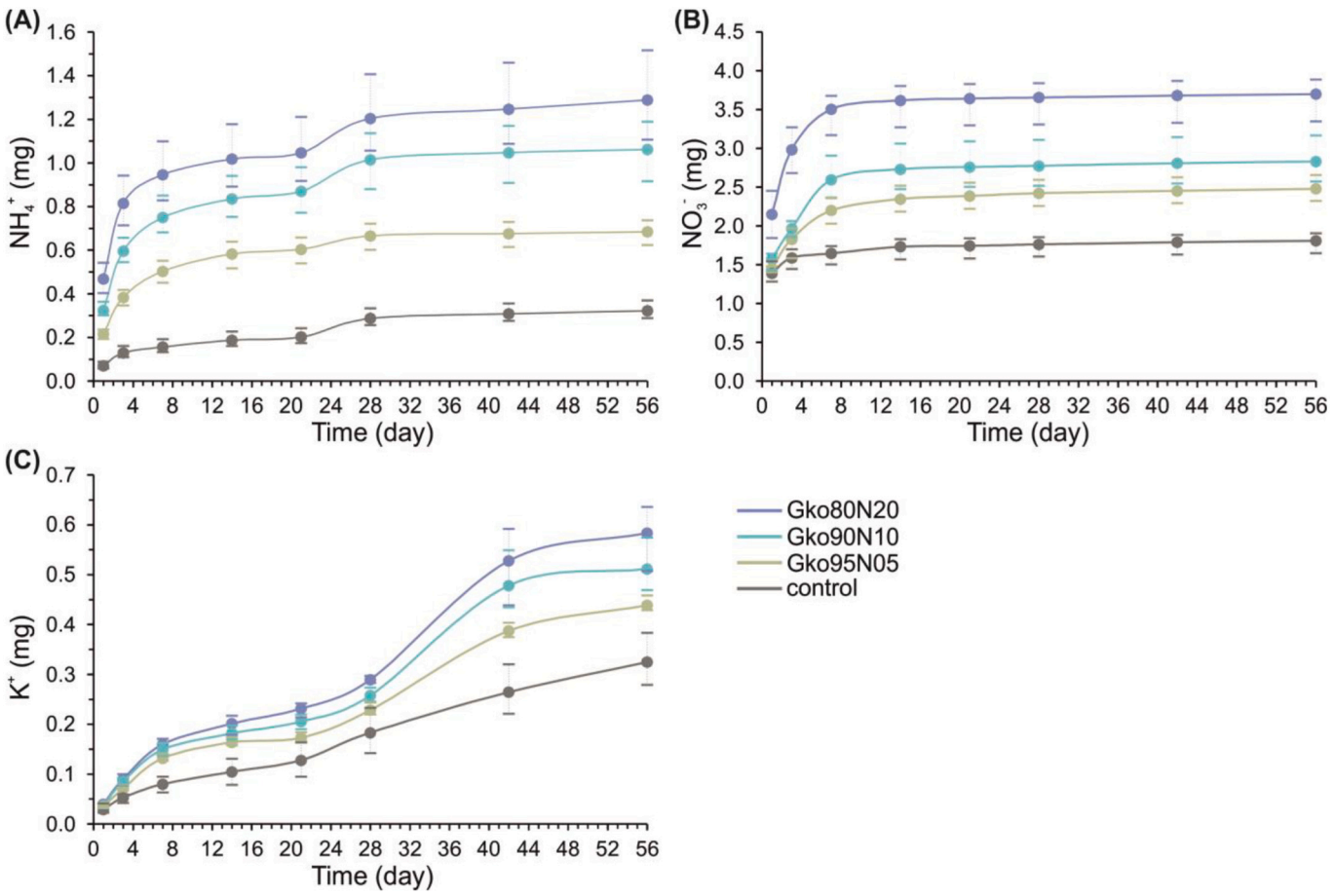

Fig. 6. Cumulative release plots of ammonium (A), nitrate (B), and potassium (C) from nanocomposites compared to a control cell without nanocomposites from laboratory tests. Dashes show minimum and maximum cumulative values. The statistical significance of every parameter indicates at the $p = 0.05$ level. Error bars represent standard deviations.

2019, 2020b, 2022a), smectite (Kim et al., 2011; Golbashy et al., 2017; Dou and Xie, 2022; Rudmin et al., 2022b; Rukchonlatee and Siriphannon, 2023) or kaolinite (Rutkai et al., 2009; Makó et al., 2019) was studied with initial destruction of the aggregated (including globular for glauconite) form of the mineral by mechanochemical preparation. What makes this study different is the use of the globular form of glauconite to trace the possible incorporation of carbamide into the interlayer spaces (micropores) during the mineral-solution interaction. That is an almost natural process of glauconite functioning, which that realised by adding of globular glauconite concentrate on the solution-gel carbamide.

In activated nanocomposites, the fraction of intercalated nitrogen mixtures is evaluated by the first basal XRD reflex shift to 15.6–17.0 Å (Fig. 1), the linear dimensions of inter-planar distance expansion on TEM images (Fig. 2), and the weight loss in the temperature range 325–590 °C with fixation of nitrogen compound release by TG-DSC-MS data (Fig. 4). As the nitrogen concentration in the reacted solution increased relative to the fraction of glauconite concentrate from 5 to 20 mol%, the intercalated portion of the nutrients increased from 2.5% (Gko95N05 nanocomposite) to 8.0% (Gko80N20 nanocomposite). The maximum intercalated portion does not exceed the proportion of the smectite layers in the glauconite package, showing the intercalating ability of the inter-planar spaces of the smectite phases specifically (Kim et al., 2011; López-Quirós et al., 2020; Rudmin et al., 2020b, 2022a). Perhaps, because of ionic exchange between ammonium and solvate water, sodium, and calcium of the original mineral. As a result, calcium and sodium are practically not fixed in the nanocomposites, with a sustained proportion of the major elements (Si, Al, Fe, Mg, K) relative to the original mineral. Thus, the intercalating ability of glauconite is determined by the number of smectite layers in its composition by the degree of its discreteness (Rieder et al., 1988; V.A. Drits et al., 2010a; Ivanovskaya et al., 2017) or maturity (Odin and Matter, 1981), as determined by geological conditions of deposit formation (Amorosi et al., 2007; Banerjee et al., 2012; López-Quirós et al., 2019).

Absorbed nitrogen compounds in the meso- and macropores are identified by IR peaks (Fig. 3) 1155 (NH_2), 1680 (NH), 3342 (NH), and 3442 (NH_2) 1/cm, mass losses between 100 and 185 °C (macropores) and 185–325 °C (mesopores) with detection of NH_3 and CO_2 ions and NH_3, CO_2, $HNCO^+$, CO^+, NH^+, NO^+, respectively (Fig. 4). The meso- and macro-pore filling is confirmed by a gradual decrease in the total pore volume from 0.064 cm^3/g in the original globular glauconite to 0.036 cm^3/g in the Gko80N20 nanocomposite and the average pore diameter from 8.9 nm to 4.1 nm. The specific surface progressively decreases the fraction of nitrogen in the initial solution increases.

A distinctive near-surface microlayer in glauconite globules (Fig. 5), presented simultaneously with oriented microscales, is a positive morphological feature of the mineral. The increased fraction of nitrogen in the near-surface microlayers shows its increased filtration capacity. It assumed that carbamide is absorbed into glauconite globules primarily because of the functioning of this solution-conducting microlayers and next penetrates the globule core. In the core part, intercalation of nitrogen compounds into the interlayer space of smectite layers of glauconite packages and absorption in the mesopore space occurs. The increased fraction of nitrogen in the near-surface microlayer relative to the core part with chaotically oriented flakes shows better intensive absorption occurs in the near-surface microlayer of globules, probably because of the presence of macropores.

4.2. Nutrient releases of glauconite-carbamide nanocomposites

The nutrient releases (ammonium, nitrate, and potassium) show a stepwise kinetic related to their interaction with the mineral (Fig. 6). The stepwise kinetics of nutrient leaching demonstrate their various presence in the nanocomposites. It assumed that easily available forms are associated with adsorbed substances in macropores, which are removed from nanocomposites in the first stages from day 1 to day 21 or from day 1 to day 7, corresponding to ammonium and nitrate, respectively. Then there is a mobilisation of absorbed ammonium from the mesopore space in the stage from the 21st to the 28th day. On the 28th day of nanocomposite activity in the soil, it removed the intercalated ammonium from the interlayer space of the mineral. The stepwise kinetics of the nutrient releases, especially ammonium and potassium, confirm the double positive function of layered glauconite in nanocomposites like both an ammonium inhibitor and a source of potassium.

Studies of mixtures based on urea or mono-ammonium phosphate and minerals revealed similar results relating to slow ammonium release due to glauconite (Rudmin et al., 2022a), smectite (Pereira et al., 2015; Golbashy et al., 2017; Baldanza et al., 2018; Gu et al., 2019; Hermida and Agustian, 2019; Silva et al., 2020; Rudmin et al., 2022b), kaolinite (Borges et al., 2015; Al-Rawajfeh et al., 2019), vermiculite (De Oliveira et al., 2021), or zeolite (Ahmad et al., 2021). Mechanical activation of glauconite-urea mixtures achieved a two-step release of ammonium and nitrate from the nanocomposites (Rudmin et al., 2022a). Another example with a mixture of urea with zeolites which also released ammonium in the first week and nitrates in the first days in a podzolic soil (Ahmad et al., 2021), with a mixture of smectite-urea, ammonium maximum is leached in the first 7–10 days (Pereira et al., 2017).

The mineral nanocomposites obtained by chemical activation of globular glauconite with carbamide have several advantages: they keep a micro-granular mineral form, have a diffusive inner microlayer, incubate nitrogen substances in micro-, meso- and macropores, and serve as a source of potassium. Furthermore, maximum ammonium intercalation occurs at an optimum glauconite: nitrogen ratio of 4:1. Ammonium intercalates in the smectite layers of mineral packages, so it is necessary to understand the degree of glauconite structural order.

5. Conclusions

As a result of the investigations conducted on the activation of globular glauconite and carbamide, the following conclusions were obtained.

1. Nitrogen intercalation occurs in the interlayer spaces (micropores) of smectite layers of glauconite. The proportion of intercalated nitrogen increases to 8% as the nitrogen concentration in the initial solution increases. A carbamide solution with 20% nitrogen concentration allows for achieving maximum intercalation.
2. Absorbed carbamide in meso- and macropores is reflected in increased specific surface area, decreased total volume, and average pore size in nanocomposites.
3. Glauconite nanocomposites keep globular particle morphology and a distinctive near-surface microlayer. The increased fraction of nitrogen in the surface microlayers shows its high filtration capacity. The surface micro-layer performs a solute-supplying function for the core part of glauconite globules.
4. The nanocomposites have a stepwise pattern of nutrient release, confirming the different carbamide absorption in glauconite micro-, meso-, and macropores. In addition, potassium, besides nitrogen compounds, is leached out of glauconite nanocomposites in stages.

Declaration of Competing Interest

The authors declare that they have no conflict of interest.

Data availability

Data will be made available on request.

Acknowledgements

The authors gratefully acknowledge the financial support provided by Russian Science Foundation through the research project № 22-77-10002.

References

Abramova, E., Lapides, I., Yariv, S., 2007. Thermo-XRD investigation of monoionic montmorillonites mechanochemically treated with urea. J. Therm. Anal. Calorim. 90, 99–106. https://doi.org/10.1007/s10973-007-8482-0.

Ahmad, A., Ijaz, S.S., He, Z., 2021. Effects of Zeolitic Urea on Nitrogen Leaching (NH4-N and NO3-N) and Volatilization (NH3) in Spodosols and Alfisols. Water 13, 1921. https://doi.org/10.3390/w13141921.

Akiyama, H., Yan, X., Yagi, K., 2010. Evaluation of effectiveness of enhanced-efficiency fertilizers as mitigation options for N2O and NO emissions from agricultural soils: Meta-analysis. Glob. Chang. Biol. 16, 1837–1846. https://doi.org/10.1111/j.1365-2486.2009.02031.x.

Al-Rawajfeh, A.E., AlShamaileh, E.M., Alrbaihat, M.R., 2019. Clean and efficient synthesis using mechanochemistry: Preparation of kaolinite–KH2PO4 and kaolinite–(NH4)2HPO4 complexes as slow released fertilizer. J. Ind. Eng. Chem. 73, 336–343. https://doi.org/10.1016/j.jiec.2019.01.046.

Alrbaihat, M., AlShamaileh, E., Al-Rawajfeh, E., 2022. Environment-friendly synthesis of Feldspar-KH2PO4 complexes by mechanochemical reaction. BOHR Intern. J. Mater. Sci. Eng. 1, 1–6. https://doi.org/10.54646/bijmse.001.

Alrbaihat, M.R., 2023. Agricultural nano fertilizers: macronutrient types and applications review. Curr. Trends Geotech. Eng. Construct. 306–316 https://doi.org/10.1007/978-981-19-7358-1_26.

Alrbaihat, M.R., Al-Rawajfeh, A.E., Alshamaileh, E., 2021. A mechanochemical preparation, properties and kinetic study of kaolin-N, P fertilizers for agricultural applications. J. Mech. Behav. Mater. 30, 265–271. https://doi.org/10.1515/JMBM-2021-0028/MACHINEREADABLECITATION/RIS.

AlShamaileh, E., Alrbaihat, M., Moosa, I., Abu-Afifeh, Q., Al-Fayyad, H., Hamadneh, I., Al-Rawajfeh, A., 2022. Mechanochemical preparation of a novel slow-release fertilizer based on K2SO4-kaolinite. Agronomy 12, 3016. https://doi.org/10.3390/agronomy12123016.

Amorosi, A., Sammartino, I., Tateo, F., 2007. Evolution patterns of glaucony maturity: a mineralogical and geochemical approach. Deep-Sea Res. II Top. Stud. Oceanogr. 54, 1364–1374. https://doi.org/10.1016/j.dsr2.2007.04.006.

Bailey, S.W., 1980. Summary of recommendations of AIPEA nomenclature committee on clay minerals. Am. Mineral. 65, 1–7. https://doi.org/10.1180/claymin.1980.015.1.07.

Baldanza, V.A.R., Souza, F.G., Filho, S.T., Franco, H.A., Oliveira, G.E., Caetano, R.M.J., Hernandez, J.A.R., Ferreira Leite, S.G., Furtado Sousa, A.M., Nazareth Silva, A.L., 2018. Controlled-release fertilizer based on poly(butylene succinate)/urea/clay and its effect on lettuce growth. J. Appl. Polym. Sci. https://doi.org/10.1002/app.46858 e46858.

Banerjee, S., Chattoraj, S.L., Saraswati, P.K., Dasgupta, S., Sarkar, U., 2012. Substrate control on formation and maturation of glauconites in the Middle Eocene Harudi Formation, western Kutch, India. Mar. Pet. Geol. 30, 144–160. https://doi.org/10.1016/j.marpetgeo.2011.10.008.

Basak, B.B., Sarkar, B., Maity, A., Chari, M.S., Banerjee, A., Biswas, D.R., 2023. Low-grade silicate minerals as value-added natural potash fertilizer in deeply weathered tropical soil. Geoderma 433, 116433. https://doi.org/10.1016/J.GEODERMA.2023.116433.

Bish, D.L., Post, J.E., 1993. Quantitative mineralogical analysis using the Rietveld full-pattern fitting method. Am. Mineral. 78, 932–940.

Borges, R., Brunatto, S.F., Leitão, A.A., De Carvalho, G.S.G., Wypych, F., 2015. Solid-state mechanochemical activation of clay minerals and soluble phosphate mixtures to obtain slow-release fertilizers. Clay Miner. 50, 153–162. https://doi.org/10.1180/claymin.2015.050.2.01.

Borges, R., Prevot, V., Forano, C., Wypych, F., 2017. Design and Kinetic Study of Sustainable potential Slow-Release Fertilizer Obtained by Mechanochemical Activation of Clay Minerals and Potassium Monohydrogen Phosphate. Ind. Eng. Chem. Res. 56, 708–716. https://doi.org/10.1021/acs.iecr.6b04378.

Borges, R., Baika, L.M., Grassi, M.T., Wypych, F., 2018. Mechanochemical conversion of chrysotile/K2HPO4 mixtures into potential sustainable and environmentally friendly slow-release fertilizers. J. Environ. Manag. 206, 962–970. https://doi.org/10.1016/J.JENVMAN.2017.11.082.

Borges, R., Giroto, A.S., Guimarães, G.G.F., Reis, H.P.G., Farinas, C.S., Ribeiro, C., 2022. Asbestos cement waste treatment through mechanochemical process with KH2PO4 for its utilization in soil pH correction and nutrient delivery. Environ. Sci. Pollut. Res. 1, 1–12. https://doi.org/10.1007/S11356-021-17679-W.

Chen, L., Chen, X.L., Zhou, C.H., Yang, H.M., Ji, S.F., Tong, D.S., Zhong, Z.K., Yu, W.H., Chu, M.Q., 2017. Environmental-friendly montmorillonite-biochar composites: Facile production and tunable adsorption-release of ammonium and phosphate. J. Clean. Prod. 156, 648–659. https://doi.org/10.1016/J.JCLEPRO.2017.04.050.

De Oliveira, D.S., Jaerger, S., Marangoni, R., 2021. Mechanochemical synthesis of expanded vermiculite with urea for filler into Alginate/Collagen Spherical Capsules: a urea slow-release system. Orbital: Electron. J. Chem. 13, 124–130. https://doi.org/10.17807/orbital.v13i2.1488.

Dou, Z., Xie, X., 2022. Chitosan-montmorillonite-Fe nanocomposite hydrogel for phosphate recovery and reuse. ACS ES and T Eng. https://doi.org/10.1021/ACSESTENGG.2C00390/ASSET/IMAGES/LARGE/EE2C00390_0007.JPEG.

Drits, V.A., 1997. Isomorphous Cation distribution in Celadonites, Glauconites and Fe-illites Determined by infrared, Mössbauer and EXAFS spectroscopies. Clay Miner. 32, 153–179. https://doi.org/10.1180/claymin.1997.032.2.01.

Drits, V.A., Ivanovskaya, T.A., Sakharov, B.A., Zvyagina, B.B., Derkowski, A., Gor'kova, N.V., Pokrovskaya, E.V., Savichev, A.T., Zaitseva, T.S., 2010a. Nature of the structural and crystal-chemical heterogeneity of the Mg-rich glauconite (Riphean, Anabar Uplift). Lithol. Miner. Resour. 45, 555–576. https://doi.org/10.1134/S0024490210060040.

Drits, Victor A., Zviagina, B.B., McCarty, D.K., Salyn, A.L., 2010b. Factors responsible for crystal-chemical variations in the solid solutions from illite to aluminoceladonite and from glauconite to celadonite. Am. Mineral. 95, 348–361. https://doi.org/10.2138/am.2010.3300.

Duan, Q., Jiang, S., Chen, F., Li, Z., Ma, L., Song, Y., Yu, X., Chen, Y., Liu, H., Yu, L., 2023. Fabrication, evaluation methodologies and models of slow-release fertilizers: a review. Ind. Crop. Prod. 192, 1–22. https://doi.org/10.1016/j.indcrop.2022.116075.

Elkhlifi, Z., Kamran, M., Maqbool, A., El-Naggar, A., Ifthikar, J., Parveen, A., Bashir, S., Rizwan, M., Mustafa, A., Irshad, S., Ali, S., Chen, Z., 2021. Phosphate-lanthanum coated sewage sludge biochar improved the soil properties and growth of ryegrass in an alkaline soil. Ecotoxicol. Environ. Saf. 216, 112173 https://doi.org/10.1016/J.ECOENV.2021.112173.

Franzosi, C., Castro, L.N., Celeda, A.M., 2014. Technical Evaluation of Glauconies as Alternative Potassium Fertilizer from the Salamanca Formation, Patagonia, Southwest Argentina. Nat. Resour. Res. 23, 311–320. https://doi.org/10.1007/s11053-014-9232-1.

Fu, J., Wang, C., Chen, X., Huang, Z., Chen, D., 2018. Classification research and types of slow controlled release fertilizers (SRFs) used - a review. Commun. Soil Sci. Plant Anal. 49, 2219–2230. https://doi.org/10.1080/00103624.2018.1499757.

Golbashy, M., Sabahi, H., Allahdadi, I., Nazokdast, H., Hosseini, M., 2017. Synthesis of highly intercalated urea-clay nanocomposite via domestic montmorillonite as eco-friendly slow-release fertilizer. Arch. Agron. Soil Sci. 63, 84–95. https://doi.org/10.1080/03650340.2016.1177175.

González, M.E., Cea, M., Medina, J., González, A., Diez, M.C., Cartes, P., Monreal, C., Navia, R., 2015. Evaluation of biodegradable polymers as encapsulating agents for the development of a urea controlled-release fertilizer using biochar as support material. Sci. Total Environ. 505, 446–453. https://doi.org/10.1016/J.SCITOTENV.2014.10.014.

Gu, H., Zhang, Y., Li, X., Li, W., Huang, S., 2019. Lignin improves release behavior of slow-release fertilizers with high content of urea. J. Appl. Polym. Sci. 48238 https://doi.org/10.1002/app.48238.

Guggenheim, S., Adams, J.M., Bain, D.C., Bergaya, F., Brigatti, M.F., Drits, V.A., Formoso, M.L.L., Galan, E., Kogure, T., Stanjek, H., 2007. Summary of recommendations of nomenclature committees relevant to clay mineralogy: Report of the Association International pour l'Etude des Argiles (AIPEA) Nomenclature Committee for 2006 (Clays and Clay Minerals). Clay Clay Miner. 55, 761–772. https://doi.org/10.1346/CCMN.2007.0550611.

Hamed, M., Abdelhafez, A.A., 2020. Application of glauconite mineral as alternative source of potassium in sandy soils. Alexan. Sci. Exchange J. 41, 181–189. https://doi.org/10.21608/asejaiqjsae.2020.91326.

Heckman, J.R., Tedrow, J.C.F., 2004. Greensand as a soil amendment. Better Crops 88, 16–17.

Hermida, L., Agustian, J., 2019. Slow release urea fertilizer synthesized through recrystallization of urea incorporating natural bentonite using various binders. Environ. Technol. Innov. 13, 113–121. https://doi.org/10.1016/J.ETI.2018.11.005.

Hillier, S., 2003. Quantitative analysis of clay and other minerals in sandstones by X-Ray powder diffraction (XRPD). In: Clay Mineral Cements in Sandstones. Blackwell Publishing Ltd., Oxford, UK, pp. 213–251. https://doi.org/10.1002/9781444304336.ch11.

Huggett, J.M., 2013. Minerals: Glauconites and Green Clays. In: Reference Module in Earth Systems and Environmental Sciences. Elsevier. https://doi.org/10.1016/b978-0-12-409548-9.02893-1.

Hussien, R.A., Donia, A.M., Atia, A.A., El-Sedfy, O.F., El-Hamid, A.R.A., Rashad, R.T., 2012. Studying some hydro-physical properties of two soils amended with kaolinite-modified cross-linked poly-acrylamides. CATENA 92, 172–178. https://doi.org/10.1016/J.CATENA.2011.12.010.

IPCC, 2014. Climate Change 2014: Mitigation of Climate Change: Working Group III Contribution to the Fifth Assessment Report of the Intergovernmental Panel on Climate Change.

Ivanovskaya, T.A., Zviagina, B.B., Zaitseva, T.S., 2017. Secondary alterations of globular and platy phyllosilicates of the glauconite–illite series in the Precambrian and Vendian–Cambrian rocks. Lithol. Miner. Resour. 52, 369–391. https://doi.org/10.1134/S0024490217050042.

Jariwala, H., Santos, R.M., Lauzon, J.D., Dutta, A., Wai Chiang, Y., 2022. Controlled release fertilizers (CRFs) for climate-smart agriculture practices: a comprehensive review on release mechanism, materials, methods of preparation, and effect on environmental parameters. Environ. Sci. Pollut. Res. 2022, 1–14. https://doi.org/10.1007/s11356-022-20890-y.

Karimi, E., Abdolzadeh, A., Sadeghipour, H.R., Aminei, A., 2012. The potential of glauconitic sandstone as a potassium fertilizer for olive plants. Arch. Agron. Soil Sci. 58, 983–993. https://doi.org/10.1080/03650340.2011.557369.

Kim, K.S., Park, M., Lim, W.T., Komarneni, S., 2011. Massive Intercalation of Urea in Montmorillonite. Soil Sci. Soc. Am. J. 75, 2361–2366. https://doi.org/10.2136/sssaj2010.0453.

Komariah, R.N., Krishanti, N.P.R.A., Yoshimura, T., Umemura, K., 2022. Characterization of Particleboard using the inner part of Oil Palm trunk (OPT) with a Bio-based Adhesive of Sucrose and ammonium Dihydrogen Phosphate (ADP). BioResources 17, 5190–5206. https://doi.org/10.15376/BIORES.17.3.5190-5206.

Lawrencia, D., Wong, S.K., Low, D.Y.S., Goh, B.H., Goh, J.K., Ruktanonchai, U.R., Soottitantawat, A., Lee, L.H., Tang, S.Y., 2021. Controlled Release Fertilizers: a Review on Coating Materials and Mechanism of Release. Plants 10, 238. https://doi.org/10.3390/plants10020238.

Lei, Z., Cagnetta, G., Li, X., Qu, J., Li, Z., Zhang, Q., Huang, J., 2018. Enhanced adsorption of potassium nitrate with potassium cation on H3PO4 modified kaolinite and nitrate anion into Mg-Al layered double hydroxide. Appl. Clay Sci. 154, 10–16. https://doi.org/10.1016/J.CLAY.2017.12.040.

Liu, J., Yang, Y., Gao, B., Li, Y.C., Xie, J., 2019. Bio-based elastic polyurethane for controlled-release urea fertilizer: Fabrication, properties, swelling and nitrogen release characteristics. J. Clean. Prod. 209, 528–537. https://doi.org/10.1016/J.JCLEPRO.2018.10.263.

Liu, Q., Liu, Y., Hao, X., Song, C., Zong, Y., Zhang, D., Shi, X., Li, P., 2023. Effects of controlled-release fertilizer on N2O emissions in wheat under elevated CO2 concentration and temperature. Plant Soil 3, 1–19. https://doi.org/10.1007/S11104-023-05972-1/FIGURES/6.

Liu, Y., Wang, J., Chen, H., Cheng, D., 2022. Environmentally friendly hydrogel: a review of classification, preparation and application in agriculture. Sci. Total Environ. 846, 157303 https://doi.org/10.1016/J.SCITOTENV.2022.157303.

López-Quirós, A., Escutia, C., Sánchez-Navas, A., Nieto, F., Garcia-Casco, A., Martín-Algarra, A., Evangelinos, D., Salabarnada, A., 2019. Glaucony authigenesis, maturity and alteration in the Weddell Sea: an indicator of paleoenvironmental conditions before the onset of Antarctic glaciation. Sci. Rep. 9, 13580. https://doi.org/10.1038/s41598-019-50107-1.

López-Quirós, A., Sánchez-Navas, A., Nieto, F., Escutia, C., 2020. New insights into the nature of glauconite. Am. Mineral. 105, 674–686. https://doi.org/10.2138/am-2020-7341.

Makó, É., Kovács, A., Kristóf, T., 2019. Influencing parameters of direct homogenization intercalation of kaolinite with urea, dimethyl sulfoxide, formamide, and N-methylformamide. Appl. Clay Sci. 182, 105287 https://doi.org/10.1016/J.CLAY.2019.105287.

Mala, R., Selvaraj, R., Sundaram, V., Rajan, R., Gurusamy, U., 2017. Evaluation of Nano Structured Slow Release Fertilizer on the Soil Fertility, Yield and Nutritional Profile of Vigna radiata. Rec. Patents Nanotechnol. 11, 50–62. https://doi.org/10.2174/1872210510666160727093554.

Mansfield, G.R., 1919. General features of the New Jersey glauconite beds. Econ. Geol. 14, 555–567.

McRae, S.G., 1972. Glauconite. Earth Sci. Rev. 8, 397–440. https://doi.org/10.1016/0012-8252(72)90063-3.

Moore, D.M., Reynolds Jr., R.C., 1997. X-Ray Diffraction and the Identification and Analysis of Clay Minerals. Oxford University Press, Oxford, UK.

Mortland, M.M., Fripiat, J.J., Chaussidon, J., Uytterhoeven, J., 1963. Interaction between ammonia and the expanding lattices of montmorillonite and vermiculite. J. Phys. Chem. 67, 248–258. https://doi.org/10.1021/J100796A009/ASSET/J100796A009.FP.PNG_V03.

Ni, B., Liu, M., Lü, S., Xie, L., Wang, Y., 2011. Environmentally Friendly Slow-Release Nitrogen Fertilizer. J. Agric. Food Chem. 59, 10169–10175. https://doi.org/10.1021/jf202131z.

Obieze, C.C., Chikere, C.B., Adeleke, R., Akaranta, O., 2019. Formulation and evaluation of slow-release fertilizer from agricultural and industrial wastes for remediation of crude oil-polluted soils. In: Society of Petroleum Engineers - SPE Nigeria Annual International Conference and Exhibition 2019. NAIC, p. 2019. https://doi.org/10.2118/198815-MS.

Odin, G.S., Matter, A., 1981. De glauconiarum origine. Sedimentology 28, 611–641.

Odom, I.E., 1984. Glauconite and celadonite minerals. In: Bailey, S.W. (Ed.), Micas. De Gruyter, pp. 545–572. https://doi.org/10.1515/9781501508820-017.

Oertli, J.J., 1980. Controlled-release fertilizers. Fertili. Res. 1, 103–123. https://doi.org/10.1007/BF01073182.

Oze, C., Smaill, J.B., Reid, C.M., Palin, M., 2019. Potassium and metal release related to glaucony dissolution in soils. Soil Syst. 3, 1–17. https://doi.org/10.3390/soilsystems3040070.

Pereira, E.I., da Cruz, C.C.T., Solomon, A., Le, A., Cavigelli, M.A., Ribeiro, C., 2015. Novel slow-release nanocomposite nitrogen fertilizers: the impact of polymers on nanocomposite properties and function. Ind. Eng. Chem. Res. 54, 3717–3725. https://doi.org/10.1021/acs.iecr.5b00176.

Pereira, E.I., Nogueira, A., A.R, Cruz, C.C.T., Guimarães, G.G.F., Foschini, M.M., Bernardi, A.C.C., Ribeiro, C., 2017. Controlled urea release employing nanocomposites increases the efficiency of nitrogen use by forage. ACS Sustain. Chem. Eng. 5, 9993–10001. https://doi.org/10.1021/acssuschemeng.7b01919.

Pogorzelski, D., Filho, J.F.L., Matias, P.C., Santos, W.O., Vergütz, L., Melo, L.C.A., 2020. Biochar as composite of phosphate fertilizer: Characterization and agronomic effectiveness. Sci. Total Environ. 743, 140604 https://doi.org/10.1016/j.scitotenv.2020.140604.

Praveen, S., Adhikari, T., Singh, M., Patra, A.K., Singh, R.N., 2020. Bio-extraction of Potassium from Glauconite Nano-particle in an Alfisols of Southern India. Commun. Soil Sci. Plant Anal. 1–15 https://doi.org/10.1080/00103624.2020.1798984.

Pretty, J., Sutherland, W.J., Ashby, J., Auburn, J., Baulcombe, D., Bell, M., Bentley, J., Bickersteth, S., Brown, K., Burke, J., Campbell, H., Chen, K., Crowley, E., Crute, I., Dobbelaere, D., Edwards-Jones, G., Funes-Monzote, F., Godfray, H.C.J., Griffon, M., Gypmantisiri, P., Haddad, L., Halavatau, S., Herren, H., Holderness, M., Izac, A.-M., Jones, M., Koohafkan, P., Lal, R., Lang, T., McNeely, J., Mueller, A., Nisbett, N., Noble, A., Pingali, P., Pinto, Y., Rabbinge, R., Ravindranath, N.H., Rola, A., Roling, N., Sage, C., Settle, W., Sha, J.M., Shiming, L., Simons, T., Smith, P., Strzepeck, K., Swaine, H., Terry, E., Tomich, T.P., Toulmin, C., Trigo, E., Twomlow, S., Vis, J.K., Wilson, J., Pilgrim, S., 2010. The top 100 questions of importance to the future of global agriculture. Int. J. Agric. Sustain. 8, 219–236. https://doi.org/10.3763/ijas.2010.0534.

Puspita, A., Pratiwi, G., Fatimah, I., 2017. Chitosan-modified smectite clay and study on adsorption-desorption of urea. Chem. Eng. Trans. 56, 1645–1650. https://doi.org/10.3303/CET1756275.

Rahman, M.H., Haque, K.M.S., Khan, M.Z.H., 2021. A review on application of controlled released fertilizers influencing the sustainable agricultural production: a cleaner production process. Environ. Technol. Innov. 23, 101697 https://doi.org/10.1016/j.eti.2021.101697.

Rashid, M., Hussain, Q., Khan, K.S., Alwabel, M.I., Hayat, R., Akmal, M., Ijaz, S.S., Alvi, S., Obaid-ur-Rehman, 2021. Carbon-based slow-release fertilizers for efficient nutrient management: synthesis, applications, and future research needs. J. Soil Sci. Plant Nutr. 1–26 https://doi.org/10.1007/s42729-021-00429-9.

Rashidzadeh, A., Olad, A., 2014. Slow-released NPK fertilizer encapsulated by NaAlg-g-poly(AA-co-AAm)/MMT superabsorbent nanocomposite. Carbohydr. Polym. 114, 269–278. https://doi.org/10.1016/J.CARBPOL.2014.08.010.

Rieder, M., Cavazzini, G., D'yakonov, Y.S., Frank-Kamenetskii, V.A., Gottardi, G., Guggenheim, S., Koval, P.V., Müller, G., Neiva, A.M.R., Radoslovich, E.W., Robert, J.-L., Sassi, F.P., Takeda, H., Weiss, Z., Wones, D.R., 1988. Nomenclature of the micas. Can. Mineral. 36, 905–912.

Rudmin, M., Abdullayev, E., Ruban, A., Buyakov, A., Soktoev, B., 2019. Mechanochemical preparation of slow release fertilizer based on glauconite–urea complexes. Minerals 9, 507. https://doi.org/10.3390/min9090507.

Rudmin, M., Banerjee, S., Makarov, B., 2020a. Evaluation of the effects of the application of glauconitic fertilizer on oat development: a two-year field-based investigation. Agronomy 10, 872. https://doi.org/10.3390/agronomy10060872.

Rudmin, M., Banerjee, S., Yakich, T., Tabakaev, R., Ibraeva, K., Buyakov, A., Soktoev, B., Ruban, A., 2020b. Formulation of a slow-release fertilizer by mechanical activation of smectite/glauconite and urea mixtures. Appl. Clay Sci. 196, 105775 https://doi.org/10.1016/j.clay.2020.105775.

Rudmin, M., Banerjee, S., Makarov, B., Belousov, P., Kurovsky, A., Ibraeva, K., Buyakov, A., 2022a. Glauconite-urea nanocomposites as polyfunctional controlled-release fertilizers. J. Soil Sci. Plant Nutr. 22, 4035–4046. https://doi.org/10.1007/s42729-022-01006-4.

Rudmin, M., Banerjee, S., Makarov, B., Ibraeva, K., Konstantinov, A., 2022b. Mechanical activation of smectite-based nanocomposites for creation of smart fertilizers. Appl. Sci. 12, 1–11. https://doi.org/10.3390/APP12020809.

Rukchonlatee, S., Siriphannon, P., 2023. Facile preparation of montmorillonite/crosslinked chitosan containing potassium nitrate nanocomposites as eco-friendly slow release fertilizers. J. Polym. Environ. 1–12 https://doi.org/10.1007/s10924-023-02815-z.

Rutkai, G., Makó, É., Kristóf, T., 2009. Simulation and experimental study of intercalation of urea in kaolinite. J. Colloid Interface Sci. 334, 65–69. https://doi.org/10.1016/j.jcis.2009.03.022.

Said, A., Zhang, Q., Qu, J., Liu, Y., Lei, Z., Hu, H., Xu, Z., 2018. Mechanochemical activation of phlogopite to directly produce slow-release potassium fertilizer. Appl. Clay Sci. 165, 77–81. https://doi.org/10.1016/J.CLAY.2018.08.006.

Salimi, M., Motamedi, E., Safari, M., Motesharezedeh, B., Motesharezadeh, B., 2021. Synthesis of urea slow-release fertilizer using a novel starch-g-poly(styrene-co-butylacrylate) nanocomposite latex and its impact on a model crop production in greenhouse. J. Clean. Prod. 322, 129082 https://doi.org/10.1016/J.JCLEPRO.2021.129082.

Santos, W.O., Mattiello, E.M., Vergutz, L., Costa, R.F., 2016. Production and evaluation of potassium fertilizers from silicate rock. J. Plant Nutr. Soil Sci. 179, 547–556. https://doi.org/10.1002/jpln.201500484.

Sharma, G.C., 1979. Controlled-release fertilizers and horticultural applications. Sci. Hortic. 11, 107–129. https://doi.org/10.1016/0304-4238(79)90037-2.

Sharma, N., Singh, A., Dutta, R.K., 2021. Biodegradable fertilizer nanocomposite hydrogel based on poly(vinyl alcohol)/kaolin/diammonium hydrogen phosphate (DAhP) for controlled release of phosphate. Polym. Bull. 78, 2933–2950. https://doi.org/10.1007/S00289-020-03252-X/TABLES/1.

Shekhar, S., Mishra, D., Agrawal, A., Sahu, K.K., 2017. Physical and chemical characterization and recovery of potash fertilizer from glauconitic clay for agricultural application. Appl. Clay Sci. 143, 50–56. https://doi.org/10.1016/j.clay.2017.03.016.

Silva, I.A., Silva, D.S., Sousa, M.U., Menezes, R.R., Ferreira, H.S., Neves, G.A., 2020. Encapsulation of nitrogen fertilizers in mixtures with organoclays for controlled release. Clean Techn. Environ. Policy 1, 3. https://doi.org/10.1007/s10098-020-01967-z.

Singla, R., Alex, T.C., Kumar, R., 2020. On mechanical activation of glauconite: Physicochemical changes, alterations in cation exchange capacity and mechanisms. Powder Technol. 360, 337–351. https://doi.org/10.1016/j.powtec.2019.10.035.

Solihin, Zhang, Tongamp, W., Saito, F., 2011. Mechanochemical synthesis of kaolin–KH2PO4 and kaolin–NH4H2PO4 complexes for application as slow release fertilizer. Powder Technol. 212, 354–358. https://doi.org/10.1016/J.POWTEC.2011.06.012.

Syrchina, N.V., Pilip, L.V., Ashikhmina, T.Y., Kantor, G.Y., 2022. Effect of Glauconite-Containing Wastes Obtained during Phosphorite Enrichment on Lead Mobility in Soils. Biol. Bull. 49, 2004–2008. https://doi.org/10.1134/S1062359022100387.

Taylor, J.C., 1991. Computer Programs for Standardless Quantitative Analysis of Minerals using the Full Powder Diffraction Profile. Powder Diffract. 6, 2–9. https://doi.org/10.1017/S0885715600016778.

Tilman, D., Cassman, K.G., Matson, P.A., Naylor, R., Polasky, S., 2002. Agricultural sustainability and intensive production practices. Nature 418, 671–677. https://doi.org/10.1038/nature01014.

Trenkel, M.E., 1997. Controlled-Release and Stabilized Fertilizers in Agriculture. International Fertilizer Industry Association, Paris, France.

Trenkel, M.E., 2010. Slow- and Controlled-Release and Stabilized Fertilizers: An Option for Enhancing Nutrient Use Efficiency in Agriculture. International Fertilizer Industry Association (IFA), Paris, France.

Wang, C., Luo, D., Zhang, X., Huang, R., Cao, Y., Liu, G., Zhang, Y., Wang, H., 2022. Biochar-based slow-release of fertilizers for sustainable agriculture: a mini review. Environ. Sci. Ecotechnol. 10, 100167 https://doi.org/10.1016/J.ESE.2022.100167.

Wu, J., Wei, Y., Lin, J., Lin, S., 2003. Study on starch-graft-acrylamide/mineral powder superabsorbent composite. Polymer 44, 6513–6520. https://doi.org/10.1016/S0032-3861(03)00728-6.

Xiao, Y., Peng, F., Zhang, Y., Wang, J., Zhuge, Y., Zhang, S., Gao, H., 2019. Effect of bag-controlled release fertilizer on nitrogen loss, greenhouse gas emissions, and nitrogen applied amount in peach production. J. Clean. Prod. 234, 258–274. https://doi.org/10.1016/J.JCLEPRO.2019.06.219.

Zhao, X., Qi, X., Chen, Q., Ao, X., Guo, Y., 2020. Sulfur-modified coated slow-release fertilizer based on castor oil: synthesis and a controlled-release model. ACS Sustain. Chem. Eng. https://doi.org/10.1021/acssuschemeng.0c06056 acssuschemeng.0c06056.

Zviagina, B.B., Drits, V.A., Sakharov, B.A., Ivanovskaya, T.A., Dorzhieva, O.V., McCarty, D.K., 2017. Crystal-chemical regularities and identification criteria in fe-bearing k-dioctahedral micas 1m from X-Ray diffraction and infrared spectroscopy data. Clay Clay Miner. 65, 234–251. https://doi.org/10.1346/CCMN.2017.064061.